

https://dspace.org/

Enhancing the Electrochemical Performance of NickelRich Layered Cathode Material NMC 622 for LithiumIon Batteries by Ultrathin Conductive CeriaSurface Coating

Itumeleng Mokhosi; Kenneth Ozoemena

WILEY-V C H VERLAG GMBH
https://hdl.handle.net/10539/46414
WOS

Downloaded from a DSpace repository. https://dspace.org/

Check for updates

EurJIC
European Journal of Inorganic Chemistry

Research Article
doi.org/10.1002/ejic.202400689

Chemistry Europe
European Chemical Societies Publishing

www.eurjic.org

Enhancing the Electrochemical Performance of Nickel-Rich Layered Cathode Material (NMC 622) for Lithium-Ion Batteries by Ultrathin Conductive Ceria-Surface Coating

Itumeleng Seotsanyana-Mokhosi[a] and Kenneth I. Ozoemena*[a]

Layered $LiNi_{0.6}Mn_{0.2}Co_{0.2}O_2$ (NMC622) has been lauded as robust and fitting candidates for the development of the next generation lithium-ion batteries for electric vehicles and other high energy demanding applications. However, widespread commercialization of NMC622 cathode material has been frustrated by its poor cycling performance which is due to structural instability. This work shows that the electrochemical performance of the NMC622 can be greatly enhanced by surface-coating with CeO_2. A commercial NMC622 is chemically modified with a very low amount of CeO_2 (~2%) to form an ultrathin CeO_2-coated NMC622 surface (NMC622-c). The coated electrode material exhibits enhanced electrochemical performance compared to its pristine counterpart, especially in terms of Li-ion diffusion kinetics and capacity retention. This enhancement has been made possible by the NMC622-c overcoming the destructive H2/H3 phase transition, reduced Ni/Li mixing, and improved ordered hexagonal structure. Improved Li diffusion rate has also been improved for long battery life. This work provides excellent insight to researchers and entrepreneurs working hard to overcome the inherent challenges of the NMC622 and related NMC layered cathode materials.

1. Introduction

Modern lifestyle, communication and mobility are greatly influencing the pace at which the world is advancing towards renewable and sustainable energy use as a way of combatting adverse effects that result from the use of fossil fuels. Recent COVID pandemic, current world politics and wars further pushed world's leaders to bring closer the dates for 100% consumption of renewable resources with great advances in hybrid electric, plug-in hybrid electric and battery electric vehicles (HEVs, PHEVs and BEVs, respectively).[1,2] These highlights need for good energy storage systems such as lithium-ion batteries (LIBs). Layered structured Ni-rich Li $Ni_{1-x-y}Co_xMn_yO_2$ (NMC) are still some of the strong contenders as LIBs cathode materials. Their high theoretical capacity, lower cost compared to the conventional $LiCoO_2$ and relatively safe performance make them desirable for energy-thirsty applications.[3,4] However, Ni-rich NMC are still riddled with many maladies, from structural instability, thermal instability at fully charged state, fast fading upon cycling, large capacity loss during the first charge-discharge cycle even at potentials lower than 4.0 V, sensitivity to environmental conditions including deterioration in ambient storage conditions.[5] All these lead to poor electrochemical performance. Many researchers have indicated structural degradation which can be caused by anisotropic strain that results in volume expansion associated with the intercalation and deintercalation of Li ions[6–8] and side reactions between the electrode materials and the electrolyte as the main contributors to these shortfalls.

Several approaches have been adopted to overcome the problems of Ni-rich NMC which include 2% weight of ceria-coating of NMC532[9] and niobium-doping of NMC811.[10] Coating improves the structural resilience and stability of NMC. It offers a physical barrier between the cathode material and the electrolyte and depending on the nature of the coating, it can also improve the conductivity of the material.[11] Metal oxides including ceria (CeO_2)[9,12,13] alumina (Al_2O_3)[14] MgO,[9] ZrO_2,[15] ZnO, V_2O_5, nano-TiO_2,[16,17] NbO[10] and others such as SiO[18] $AlPO_4$ have been used as coatings with reports of improved electrochemical performance such as high capacity, high cycling stability and good rate capability of several electrode materials. Like ceria coating or doping, alumina-based coatings/doping are of interest because of their low-cost, compatibility, and ability to enhance rate capability and capacity retention of cathode materials, including LCO, LMO and NMC.[19–25] However, unlike alumina coatings, ceria is unique as it highly conducting due its excellent oxygen storage capacity and the presence of oxygen vacancies arising from Ce^{3+} and redox process of the Ce^{3+}/Ce^{4+}.[26–28] Moreso, ceria is known for its good electrical conductivity which allows for electron transport between ceria and metal oxide.[29] For example, ceria has been used to coat some metal oxide cathode materials (such as $LiCoO_2$, $LiNi_{0.8}Co_{0.2}O_2$, $LiCo_{1/3}Ni_{1/3}Mn_{1/3}O_2$ and $LiMn_2O_4$) to improve their electrochemistry.[12,30–32] In addition, ceria-coating has been used in NMC811 to mitigate some of the inherent challenges associated with layered cathode materials, i.e., structural

[a] I. Seotsanyana-Mokhosi, K. I. Ozoemena
Molecular Sciences Institute, School of Chemistry, University of the Witwatersrand, Johannesburg 2050, South Africa
E-mail: Kenneth.ozoemena@wits.ac.za

Supporting information for this article is available on the WWW under https://doi.org/10.1002/ejic.202400689

© 2025 The Author(s). European Journal of Inorganic Chemistry published by Wiley-VCH GmbH. This is an open access article under the terms of the Creative Commons Attribution License, which permits use, distribution and reproduction in any medium, provided the original work is properly cited.

© 2025 The Author(s). European Journal of Inorganic Chemistry published by Wiley-VCH GmbH

Research Article
doi.org/10.1002/ejic.202400689

instability, cycling instability due to dissolution of the transition metals, phase transition and cation mixing.[33] Many literature prefer the use of 2% ceria for coating cathode materials for Li-ion batteries.[9,34–36]

In this work, we report the first use of ultrathin film of ceria surface-coated on Ni-rich layered cathode material, using NMC622 as a model sample. The effects of the surface-coating on the physico-chemistry and electrochemical properties of the NMC622 are interrogated. We report how a simple process of surface-coating NMC622 with ultralow amount of ceria (~2%) can significantly tune the electrochemical performance of the NMC622-based lithium-ion battery cells, including improving first cycle coulombic efficiency, cycling stability, increased capacity and capacity retention.

Experimental Section

Material and Methods

Commercial NMC622, Carbon black, polyvinylidene fluoride (PVDF), N-Methyl pyrrolidine (NMP) and $LiPF_6$, were used without modification while ethylene carbonate (EC). Diethyl carbonate (DEC) and dimethyl carbonate (DMC) were dried using molecular sieves before use. They were all from Shandong Gelon LIB Co. LTD. The reagents $Ce(NO_3)_3{\cdot}6H_2O$ (Sigma-Aldrich) and PVA (Sigma Aldrich), were also used without further purification. Heating was done in a programmable tube furnace where the temperature was controlled by high precise SCR power controller with $+/-1\,^{\circ}C$ accuracy and it was programmed to heat at 3 °C/min. The crystal structures were characterised using Raman spectroscopy, scanning electron microscopy (SEM) coupled with energy dispersive spectroscopy (EDS), TEM and powder X-ray diffraction (PXRD). Horiba Jobin-Yvon LabRAM HR Raman spectrometer equipped with an Olympus BX41 microscope attachment was used to obtain the Raman spectra. A Bruker D2 diffractometer 580 equipped with Cu Kα radiation (λ = 1.54178 Å and scanned within range 10°–90° at a scanning rate of 2.7°/min was employed to identify the XRD crystal structure. The morphology of the powders was studied using the Zeiss SEM and TEM microscopes and the elemental content of the powders were studied using EDS in conjunction with SEM.

Electrochemical tests were carried out as half-cell measurements using R2032 coin cells. Typically, cathode electrodes were fabricated from an 8:1:1 mass ratio of the cathode material to PVDF binder to carbon black. First the binder was placed in an agate mortar and NMP was added as the solvent and combined, then a mixture of combined cathode and carbon powders were added, and all were mixed into a slurry. The prepared slurry was evenly applied onto an aluminum foil current collector using a coating machine. The coated sheet was placed in a vacuum oven at 120 °C overnight to dry before calendaring. The coated electrode sheet was then cut into 12 mm diameter discs and transferred to an argon-filled MBraun glovebox for cell fabrication. The R2032 coin cells were assembled in an argon-filled glovebox using the coated cathode discs, lithium foil discs as an anode, 1 M $LiPF_6$ in EC/DEC/DMC (1:1:1 volume ratio) as the electrolyte and micro-porous polypropylene Celgard H1612/16 μm as the separator. The electrochemical measurements were carried out on a BioLogic system (BCS-800 series). A BT-Lab program was used for data acquisition and analysis.

Experimental

Synthesis of 2% CeO_2-coated NMC622 by mass was made by weighing out enough $Ce(NO_3)_3{\cdot}6H_2O$ to contribute the Ce^{3+} ions for a 2% CeO_2 by mass of the commercial NMC622 (summarized in Figure 1).

The nitrate salt was then dissolved in deionised water and the weighed NMC622 was added and dispersed in an ultrasound sonicator bath. Polyvinyl alcohol (PVA) was stirred into the mixture. The resultant suspension was left to dry in a vacuum oven at 80 °C. The dry residue was crushed in an agate mortar and pestle before

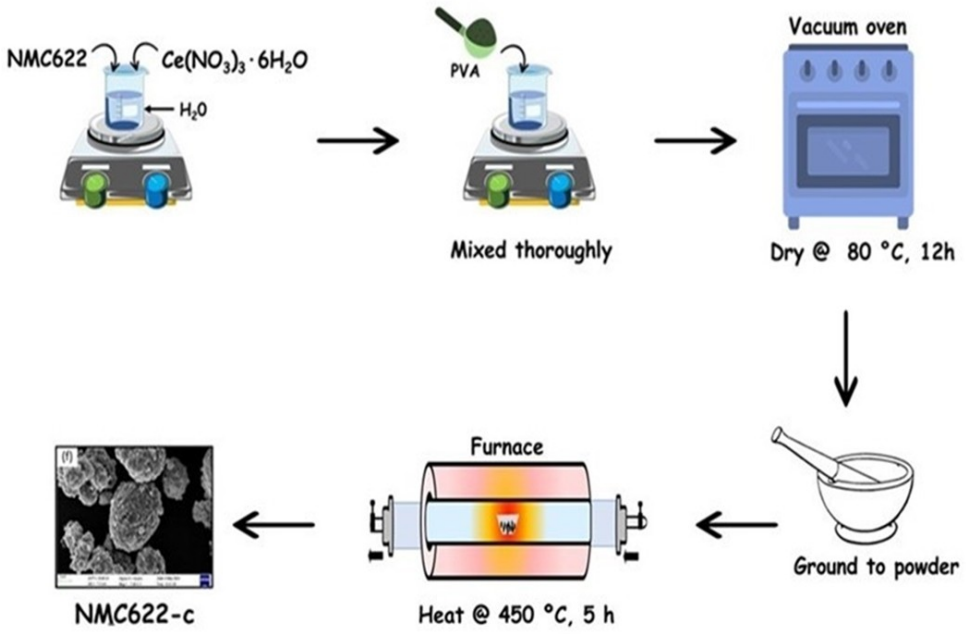


Figure 1. Schematic of the synthesis method of NMC622-c.

© 2025 The Author(s). European Journal of Inorganic Chemistry published by Wiley-VCH GmbH

10990682c, 2025, 10, Downloaded from https://chemistry-europe.onlinelibrary.wiley.com/doi/10.1002/ejic.202400689 by University Of Witwatersrand, Wiley Online Library on [30/07/2025]. See the Terms and Conditions (https://onlinelibrary.wiley.com/terms-and-conditions) on Wiley Online Library for rules of use; OA articles are governed by the applicable Creative Commons License

Research Article
doi.org/10.1002/ejic.202400689

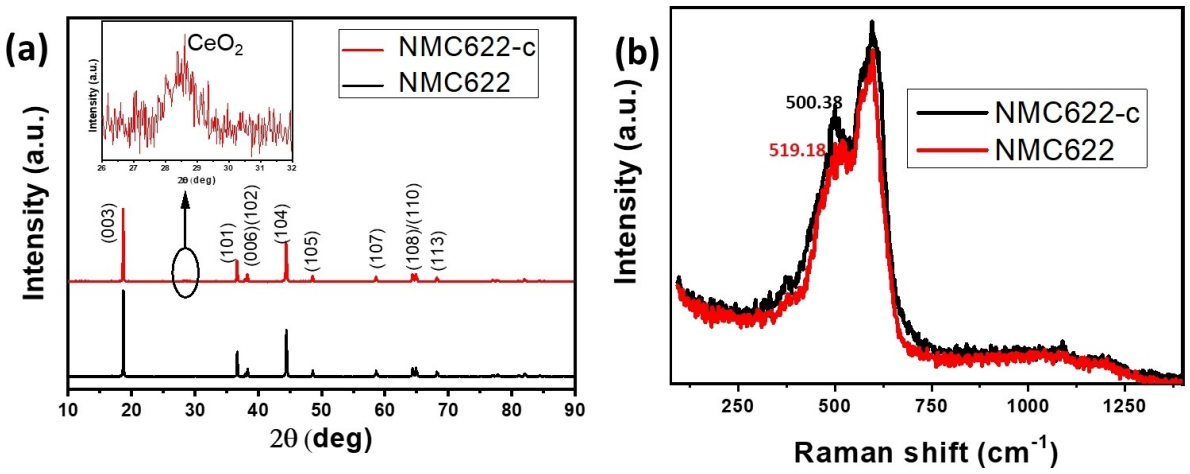


Figure 2. (a) XRD patterns of NMC622 and NMC622-c and the insert show the expanded area between 27–32° and (b) Raman spectra of NMC622-c and NMC622.

treating with heat at 450 °C for 5 h in a tube furnace. The NMC622-c powder was cooled and ground into a powder.

2. Results and Discussion

2.1. Phase and Morphology Analysis

The powder XRD pattern of NMC622 and coated NMC622-c captured between 5–90° is shown in Figure 2. They both have a typical $LiMO_2$ structure of $\alpha NaFeO_2$ layered structure with a R3 m space group that has been indexed to hexagonal lattice (JCPDS No. 00–066-0854) with the atoms Li, M (M═Ni, Mn, Co) and O, at 3a, 3b and 6c sites as describe for NMC111.[4] The peaks are sharp and with high intensity proving that the particles are crystalline and thus have structural periodicity. The highly crystalline materials show a clear separation of the peaks in the doublets of (006)/(102) and (018)/(110) which is characteristic of highly ordered layered structure that is free from impurities.[3]

Crystalline CeO_2 is a highly refractive material. The fact that strong fingerprint peaks on the pattern due to CeO_2 are missing suggests that it did not form as a crystalline material and the amount was small. Previous work showed that XRD of a coated material may or may not result in extra peaks of the coating material depending on the amount of the coat added[3,13] and the temperature used to apply the coat. Often temperatures above 700 °C, are needed to insert an atom into the host lattice,[13] and this will most likely also cause some shifts in the peak positions of the host material. The peak positions are similar for both materials except for the weak signal at ~28.6° as shown in the insert in Figure 2. This signal is produced by CeO_2 and it is broad which suggests that the coat may be lacking the close packed structural periodicity of crystalline solids. The broadness is caused by the non-coherence in the arrangement or the positioning of the atoms in the M–O frame. This suggests that the coating is amorphous, adhering to the surface of the host material and it is most likely thin layered as can be expected because of the small amount, 2 % by mass that was theoretically expected. This coating has preserved the layered structure of the bulk material which is suited for easy diffusion of the Li ions.

Table 1 shows the summary of calculations made from the XRD patterns of NMC622 and NMC622-c. with the ratio of intensity of $I_{(003)}/I_{(104)}$ being 1.85 and 1.87 for NMC622 and NMC622-c, respectively. The $I_{(003)}/I_{(104)}$ ratio >1.2 indicates absence of cationic mixing. The r_1 factor obtained by $I_{(006)}+I_{(102)}/I_{(101)}$ is an indicator of the hexagonal ordering, where $r_1 < 0.6$ signifies a distinct highly ordered hexagonal structure. This is true for both samples. Thus, the coating neither affected the ordering nor the cationic mixing. Owing to the high similarity in patterns of the NMC622 and NMC622-c coating is not to expected to adversely affect the diffusion of Li within the cathode because it did not change the layered structure of NMC622.

Figure 2(b) shows the Raman spectra of NMC622-c and NMC622 between 100 and 1000 Raman shifts. Both spectra are almost similar without an observable signal by O–Ce–O stretches which agrees with the XRD data which could be overlapping with E_g (Ni) around 460 cm^{-1}. The slight shift of the peak of the NMC622-c to lower region (i.e., from about 519–500 cm^{-1}) is indicative of surface defect. This is because of the small amount of CeO_2 formed. Both samples have strong bands between 430 and 640 cm^{-1} which are due to the Raman active A_{1g} and E_g modes of M–O and O–M–O stretches and vibrations for the Ni, Co and Mn found in this region. All six Raman active

Table 1. Cation mixing parameters and lattice parameters of NMC622 and NMC622-c.

Cathode material	Intensity ratio (I_{003}/I_{104})	r_1 factor $\frac{I_{(006)}+I_{(102)}}{I_{(102)}}$
NMC622	1.85	0.44
NMC622-c	1.87	0.42

© 2025 The Author(s). European Journal of Inorganic Chemistry published by Wiley-VCH GmbH

10990682c, 2025, 10, Downloaded from https://chemistry-europe.onlinelibrary.wiley.com/doi/10.1002/ejic.202400689 by University Of Witwatersrand, Wiley Online Library on [30/07/2025]. See the Terms and Conditions (https://onlinelibrary.wiley.com/terms-and-conditions) on Wiley Online Library for rules of use; OA articles are governed by the applicable Creative Commons License

Research Article
doi.org/10.1002/ejic.202400689

modes were not easily discernible and upon deconvolution only five signals were picked shown in Figure S1, the A_{1g}(Ni) mode could not be picked. This is another indication of little cationic mixing as Ni–O and O–Ni–O vibrations are narrower when there is more ordering and little cationic mixing of the Ni and Li atoms.[37]

Morphology of the samples was studied using SEM. Figure 3 shows the SEM images of both NMC622 and NMC622-c. NMC622 in Figure 3(a) has hexagonal particles with some rough flaky surface while Figure 3(b) shows that NMC622-c, has a smooth surface, confirming the successful application of the CeO_2 coating.

Probing by energy-dispersive X-ray spectroscopy (EDX) analysis was done on the flaky part and the hexagonal particle and it showed the presence of all expected elements. However, the data on elemental composition shows that the expected atomic and weight percentages were accurate only for the cuboid structure as listed in Table 2. Thus, the flakes seen on high magnification with SEM are most likely degradation products and their elemental composition does not match the theoretically expected one, while the theoretical elemental composition fits for the cube region. Element mapping images shows satisfactory distribution of the component elements. Figure 3e shows typical elemental mapping images of the NMC622-c, confirming that metal Ce was also evenly and selectively spread on the NMC622-c sample proving further that indeed Ce was successfully introduced onto the cathode material.

TEM imaging was carried out to further analyze the surface of the materials. Figure 4 shows the TEM images. The particles have variable macro-sized diameter of around 100–150 nm. The HRTEM image, Figure 4 (c) shows the presence of an ultra-thin layer with thickness of 6–10 nm on the surface of NMC622-c.

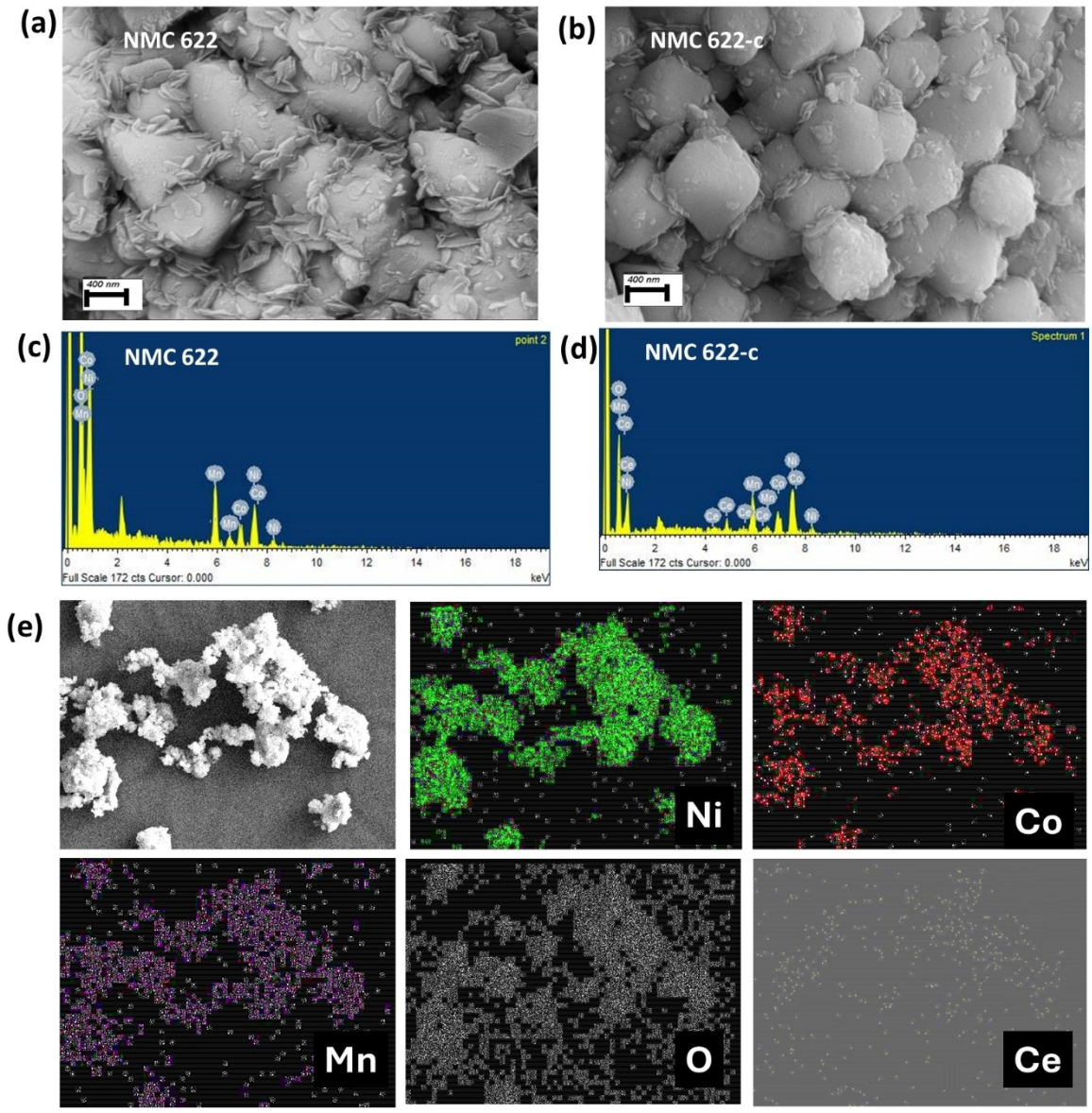


Figure 3. SEM images of (a) NMC622 and (b) NMC622-c and EDS of (c) NMC622 and (d) NMC622-c, and (e) typical elemental mapping of NMC622-c.

© 2025 The Author(s). European Journal of Inorganic Chemistry published by Wiley-VCH GmbH

10990682c, 2025, 10, Downloaded from https://chemistry-europe.onlinelibrary.wiley.com/doi/10.1002/ejic.202400689 by University Of Witwatersrand, Wiley Online Library on [30/07/2025]. See the Terms and Conditions (https://onlinelibrary.wiley.com/terms-and-conditions) on Wiley Online Library for rules of use; OA articles are governed by the applicable Creative Commons License

Research Article
doi.org/10.1002/ejic.202400689

Table 2. CV peak potentials for NMC622 and NMC622-c and for the dominant peak.

compound	*Peak potential ($E_{1/2,\ V\ vs\ Li/Li^+}$)*					
	Oxidation 1st cycle	*Reduction 1st cycle*	*$\triangle E_P$*	*Oxidation 2nd cycle*	*Reduction 2nd cycle*	*$\triangle E_P$*
NMC622	4.32 3.93	n/a 3.67	0.65 0.26	3.89 n/a	3.67 n/a	0.22 n/a
NMC622-c	4.19 3.92	3.67 n/a	0.52 0.25	3.95 n/a	3.67 n/a	0.21 n/a

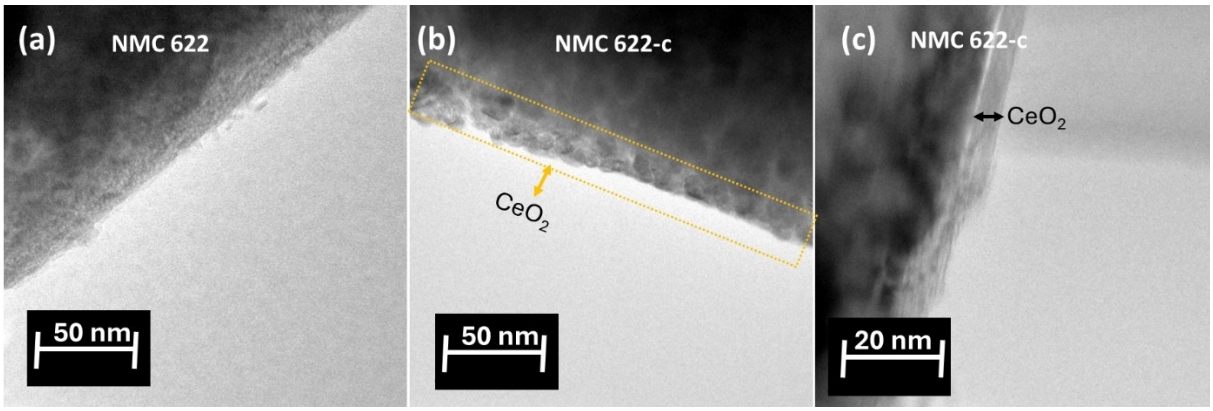


Figure 4. TEM images of (a) NMC622, (b) NMC622-c (c) HRTEM of NMC622-c.

2.2. Electrochemical Measurements

Figure 5(a) shows the cyclic voltammograms of two NMC powders were measured in half cells between 2.8 and 4.4 V in 1 M LiPF6 in EC/DEC/DMC (1 : 1 : 1 volume ratio) at 0.1 mV/s scan rate. On first scan, two oxidation processes were observed for NMC622 with half wave potentials of $E_{1/2} = 3.93$ and 4.32 V vs Li/Li^+ for process I and II, respectively and has been summarized in Table 2. However, on reduction, a single dominant process was seen at half wave potential of $E_{1/2} = 3.67$ V and two smaller processes show as indistinct humps at $E_{1/2} = 3.92$ and at $E_{1/2} = 4.18$ V vs Li/Li^+. Similarly in the first cycle NMC622-c has two oxidation peaks, a low current peak at $E_{1/2} = 4.19$ vs Li/Li^+ and a dominant peak at $E_{1/2} = 3.92$ V still with one reduction peak at $E_{1/2} = 3.67$ V vs. Li/Li^+. The process at high voltage is quasi-reversible reactions responsible for multiphase transitions between two hexagonal structures (H2–H3).[38,39] The H2–H3 phase transitions are caused by $Ni^{2+/4+}$ processes. There is a large charge difference between the Ni^{2+} and Ni^{4+} ions they can lead to catastrophic volume contraction leading to Ni loss resulting in structural degradation and capacity fading. Although both samples exhibit the H2–H3 phase transitions according to the Figure, it is more pronounced in uncoated NMC622 than in NMC622-c.

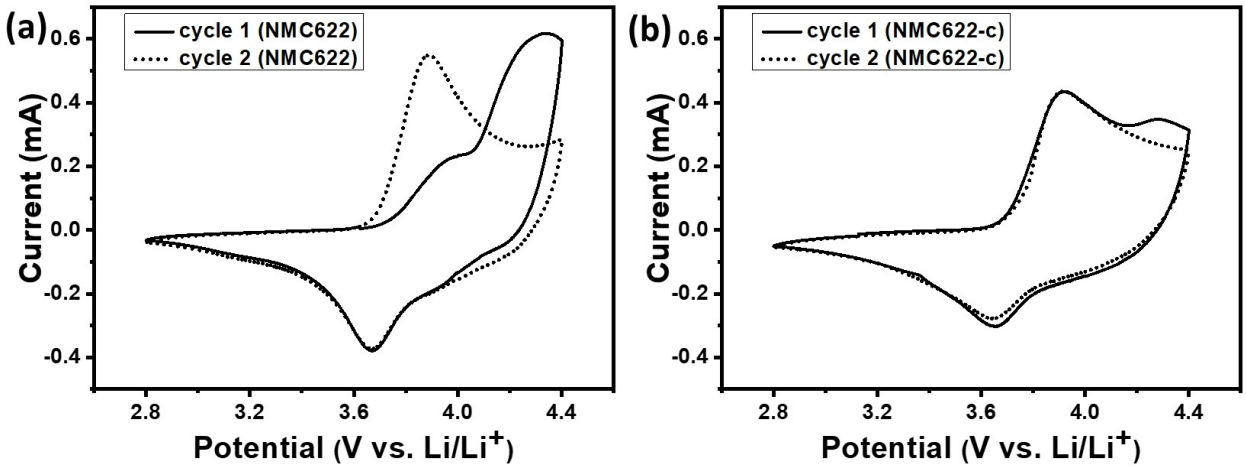


Figure 5. Comparative cyclic voltammograms of (a) NMC622 and (b) NMC622-c conducted at 0.1 $mV\,s^{-1}$.

© 2025 The Author(s). European Journal of Inorganic Chemistry published by Wiley-VCH GmbH

10990682c, 2025, 10, Downloaded from https://chemistry-europe.onlinelibrary.wiley.com/doi/10.1002/ejic.202400689 by University Of Witwatersrand, Wiley Online Library on [30/07/2025]. See the Terms and Conditions (https://onlinelibrary.wiley.com/terms-and-conditions) on Wiley Online Library for rules of use; OA articles are governed by the applicable Creative Commons License

Research Article
doi.org/10.1002/ejic.202400689

On second cycling, the shape of the voltammogram and the peak currents changed to show a single redox couple for both NMC622 and NMC622-c. The oxidation peak is at $E_{1/2}=3.89$ and $E_{1/2}=3.95$ V for NMC622 and NMC622-c, respectively and on reverse scan both show a peak at $E_{1/2}=3.67$ V vs. Li/Li^+ for NMC622 and NMC622-c. The latter oxidation peak is at higher potential for NMC622-c proving that NMC622 exhibits faster diffusion that NMC622-c. This is expected owing to the presence of a CeO_2 coat which would lead to slower diffusion of Li ions because of greater distances the ions would have to travel, and the formation of the SEI. In general, shape of the CV curves and $\triangle E_P$ shows fast kinetics for both the uncoated NMC622 and NMC622-c with proves the good electrochemical characteristics of NMC622. Furthermore, cyclic voltammograms of NMC622 and NMC622-c had almost similar half potential as summarized in Table 2 which further indicates that an ultrathin layer of CeO_2 does not totally block the electrochemical processes of NMC 622.

Long-term galvanostatic charge-discharge cycling experiments (up to 50 cycles) at 0.1 C, (1 C = 270 mA hg^{-1}) were conducted for the two cells between the potential window of 2.8–4.3 V at room temperature (Figure 6a & b). The NMC622 cell showed first cycle capacity loss of about 37% while the NMC622-c lost about 63%. The pristine NMC622 (Figure 6a) delivers more discharge capacity of ~205 mA hg^{-1} while NMC622-c (Figure 6b) had an initial discharge capacity of 150 mA hg^{-1} and then increased as the cycling number increased. This finding confirms the electronic interaction between the NMC and its ceria coating.

Figures 6c and d compare the capacity retention and corresponding Coulombic efficiency profiles. At the end of the 50th cycle, the pristine NMC622 lost about 18% of its initial capacity while the ceria-coated sample (NMC-c) gained about 14% capacity after a few cycles. This behaviour of the ceria-coated sample indicates activation for efficient Li diffusion, mediated by enhanced electronic interaction of the ceria and NMC. In other words, there is a gradual development of lithium ions 'highway' that improves the intercalation/deintercalation process. The coulombic efficiency (CE) for the two materials range between 97% and 100% except for the first cycle where it was 60% and 65% for NMC622 and NMC622-c, respectively. Even during the electrode activation stage, the coulombic efficiency is high. High CE is an indication of efficient operating cell with little side reactions and little loss of lithium during cycling.[40] Such cells are expected to show good cycling reversibility and run for a long time. The initial low EC is attributed to the formation of the SEI, while the less than 100% efficiency an indication of the immediate development of the SEI. This observation of the ceria-coated sample suggests that ceria-coating improves conductivity of NMC622 cathode material and limits the continued formation of the SEI layer with cycling. Also, the enhanced capacity retention of the NMC622-c further agrees with the observed shapes of the CV which showed more H2–H3 for uncoated sample than for the NMC622-c which explains the more rapid decay for NMC622.

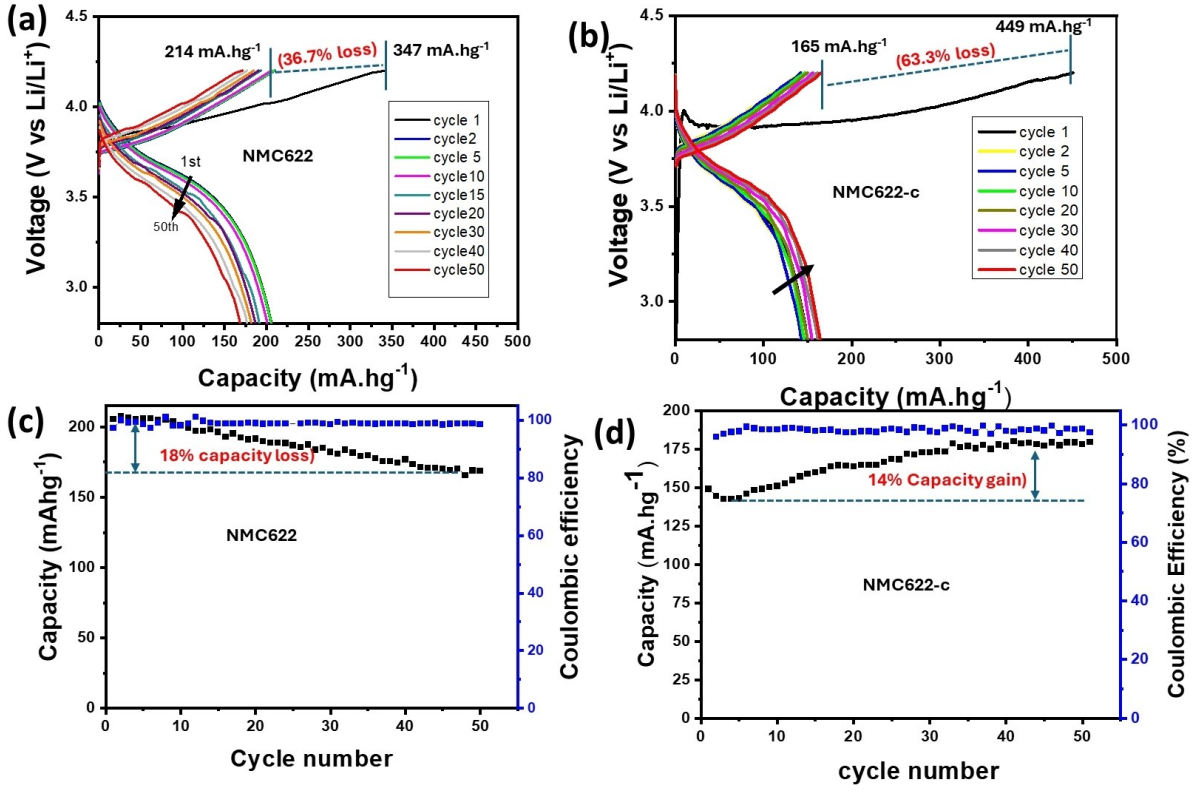


Figure 6. Comparative long-term cycling (50 cycles) of (a) NMC622 and (b) NMC622-c; Capacity retention and coulombic efficiency profiles of (c) NMC622 and (d) NMC622-c.

© 2025 The Author(s). European Journal of Inorganic Chemistry published by Wiley-VCH GmbH

10990682c, 2025, 10, Downloaded from https://chemistry-europe.onlinelibrary.wiley.com/doi/10.1002/ejic.202400689 by University Of Witwatersrand, Wiley Online Library on [30/07/2025]. See the Terms and Conditions (https://onlinelibrary.wiley.com/terms-and-conditions) on Wiley Online Library for rules of use; OA articles are governed by the applicable Creative Commons License

It is interesting to note that our synthesis strategy of 2% ceria coating of the pristine NMC gave similar or even better electrochemical properties (especially in terms of improved redox kinetics and capacity retention) that are excellently comparable to other cathode materials coated with 2% ceria.[9,34–36] For example, none of the sate-of-the-art materials, for example the NMC532,[9] recorded the excellently enhanced capacity and capacity retention as shown by NMC622-c.

3. Conclusions

Surface modification of commercial NMC622 with very low amount of ceria was successful as evident from XRD, SEM and TEM data. The ultrathin CeO_2 layer stabilized the surface of NMC622 thereby protecting it from parasitic reactions that could lead to capacity loss. The layer helps to curb the loss of capacity during first cycle by significantly blocking the H2/H3 phase transition. This overall improvement in structural stability and electrochemical properties makes ceria oxide coating a potential method to use on NMC622 to improve its performance and expand its use in energy thirsty operations and it uses very little ceria.

Acknowledgements

The authors are grateful the South Africa's National Research Foundation (NRF) and the Department of Science and Innovation for their support through the SARChI Chair program (UID no.: 132739). ISM thanks the South African Department of Trade, Industry and Competition (DTIC) for PhD bursary through Indabuko as SMME.

Conflict of Interests

The authors declare no conflict of interest.

Data Availability Statement

The data that support the findings of this study are available from the corresponding author upon reasonable request.

Keywords: Lithium-ion battery · NMC622 cathode · CeO_2-coating · Coulombic efficiency · Capacity retention

[1] L. A. Arias, E. Rivas, F. Santamaria, V. Hernandez, *Energies* **2018**, *11*(7), 1617.
[2] D. Andre, S.-J. Kim, P. Lamp, S. F. Lux, F. Maglia, O. Paschos, B. Stiaszny, *J. Mater. Chem. A* **2015**, *3*(13), 6709–6732.
[3] P. Periasamy, N. Kalaiselvi, H. Kim, *Int. J. Electrochem. Sci.* **2007**, *2*(9), 689–699.
[4] K. Shaju, G. S. Rao, B. Chowdari, *Electrochim. Acta* **2002**, *48*(2), 145–151.
[5] K. Min, K. Kim, C. Jung, S.-W. Seo, Y. Y. Song, H. S. Lee, J. Shin, E. Cho, *J. Power Sources* **2016**, *315*, 111–119.
[6] T. Krause, D. Nusko, L. Pitta Bauermann, M. Vetter, M. Schäfer, C. Holly, *Energies* **2024**, *17*(7), 1566.
[7] W. Mai, A. Colclasure, K. Smith, *J. Electrochem. Soc.* **2019**, *166*(8), A1330.
[8] A. O. Kondrakov, A. Schmidt, J. Xu, H. Geßwein, R. Mönig, P. Hartmann, H. Sommer, T. Brezesinski, J. r. Janek, *J. Phys. Chem. C* **2017**, *121*(6), 3286–3294.
[9] K. Liu, G.-L. Yang, Y. Dong, T. Shi, L. Chen, *J. Power Sources* **2015**, *281*, 370–377.
[10] F. Xin, H. Zhou, Y. Zong, M. Zuba, Y. Chen, N. A. Chernova, J. Bai, B. Pei, A. Goel, J. Rana, *ACS Energy Lett.* **2021**, *6*(4), 1377–1382.
[11] Y. Gao, R. L. Patel, K.-Y. Shen, X. Wang, R. L. Axelbaum, X. Liang, *ACS Omega* **2018**, *3*(1), 906–916.
[12] F. Wu, M. Wang, Y. Su, L. Bao, S. Chen, *Electrochim. Acta* **2009**, *54*(27), 6803–6807.
[13] R. L. Patel, J. Park, X. Liang, *RSC Adv.* **2016**, *6*(101), 98768–98776.
[14] Y. Wu, A. Manthiram, *Electrochem. Solid-State Lett.* **2006**, *9*(5), A221.
[15] J. Liu, M. Yuan, T. Xie, G. Yan, *J. Mater. Res.* **2022**, *37*(5), 1019–1029.
[16] Q. Fan, K. Lin, S. Yang, S. Guan, J. Chen, S. Feng, J. Liu, L. Liu, J. Li, Z. Shi, *J. Power Sources* **2020**, *477*, 228745.
[17] J. Zheng, J. Li, Z. Zhang, X. Guo, Y. Yang, *Solid State Ion.* **2008**, *179*(27–32), 1794–1799.
[18] X. Lu, N. Zhang, M. Jahn, W. Pfleging, H. J. Seifert, *Appl. Sci.* **2019**, *9*(18), 3671.
[19] S.-T. Myung, K. Izumi, S. Komaba, Y.-K. Sun, H. Yashiro, N. Kumagai, *Chem. Mater.* **2005**, *17*(14), 3695–3704.
[20] J. Cho, Y. J. Kim, B. Park, *Chem. Mater.* **2000**, *12*(12), 3788–3791.
[21] M. Pasqualini, S. Calcaterra, F. Maroni, S. Rezvani, A. Di Cicco, S. Alexander, H. Rajantie, R. Tossici, F. Nobili, *Electrochim. Acta* **2017**, *258*, 175–181.
[22] F. Nkosi, N. Palaniyandy, K. Raju, K. I. Ozoemena, *Electroanalysis* **2020**, *32*(12), 3159–3169.
[23] F. P. Nkosi, N. Palaniyandy, K. Raju, C. Billing, K. I. Ozoemena, *Mater. Res. Express* **2019**, *6*(11), 115501.
[24] F. P. Nkosi, C. J. Jafta, M. Kebede, L. Le Roux, M. K. Mathe, K. I. Ozoemena, *RSC Adv.* **2015**, *5*(41), 32256–32262.
[25] C. J. Jafta, K. Raju, M. K. Mathe, N. Manyala, K. I. Ozoemena, *J. Electrochem. Soc.* **2015**, *162*(4), A768.
[26] J. M. Jacob, P. G. Corradini, E. Antolini, N. A. Santos, J. Perez, *Appl. Catal., B* **2015**, *165*, 176–184.
[27] L. Artiglia, S. Agnoli, *J. Phys. Chem. C* **2018**, *122*(36), 20809–20816.
[28] R. A. Hameed, R. Amin, K. El-Khatib, A. E. Fetohi, *Appl. Surf. Sci.* **2016**, *367*, 382–390.
[29] L. Daza, C. Rangel, J. Baranda, M. Casais, M. Martınez, J. Alonso, *J. Power Sources* **2000**, *86*(1–2), 329–333.
[30] H.-W. Ha, K. H. Jeong, N. J. Yun, M. Z. Hong, K. Kim, *Electrochim. Acta* **2005**, *50*(18), 3764–3769.
[31] H.-W. Ha, N. J. Yun, K. Kim, *Electrochim. Acta* **2007**, *52*(9), 3236–3241.
[32] H.-W. Ha, N. J. Yun, M. H. Kim, M. H. Woo, K. Kim, *Electrochim. Acta* **2006**, *51*(16), 3297–3302.
[33] F. Wu, Q. Li, L. Chen, Y. Lu, Y. Su, L. Bao, R. Chen, S. Chen, *ChemSusChem* **2019**, *12*(4), 935–943.
[34] J. Yao, F. Wu, X. Qiu, N. Li, Y. Su, *Electrochim. Acta* **2011**, *56*(16), 5587–5592.
[35] M.-Y. Cho, K.-C. Roh, S.-M. Park, J.-W. Lee, *Mater. Lett.* **2011**, *65*(13).
[36] Y. Wang, J. Tang, *RSC Adv.* **2018**, *8*(43), 24143–24153.
[37] C. M. Julien, A. Mauger, *AIMS Mater. Sci.* **2018**, *5*(4), 650–698.
[38] Z. Ahaliabadeh, V. Miikkulainen, M. Mantymaki, S. Mousavihashemi, J. Lahtinen, Y. Lide, H. Jiang, K. Mizohata, T. Kankaanpaa, T. Kallio, *ACS Appl. Mater. Interfaces* **2021**, *13*(36), 42773–42790.
[39] Y. Ruan, X. Song, Y. Fu, C. Song, V. Battaglia, *J. Power Sources* **2018**, *400*, 539–548.
[40] F. Yang, D. Wang, Y. Zhao, K.-L. Tsui, S. J. Bae, *Energy* **2018**, *145*, 486–495.

Manuscript received: October 17, 2024
Revised manuscript received: February 11, 2025
Accepted manuscript online: February 20, 2025
Version of record online: March 21, 2025

© 2025 The Author(s). European Journal of Inorganic Chemistry published by Wiley-VCH GmbH

10990682c, 2025, 10, Downloaded from https://chemistry-europe.onlinelibrary.wiley.com/doi/10.1002/ejic.202400689 by University Of Witwatersrand, Wiley Online Library on [30/07/2025]. See the Terms and Conditions (https://onlinelibrary.wiley.com/terms-and-conditions) on Wiley Online Library for rules of use; OA articles are governed by the applicable Creative Commons License